International Journal of Solids and Structures 47 (2010) 1737–1750

Contents lists available at ScienceDirect

International Journal of Solids and Structures

journal homepage: www.elsevier.com/locate/ijsolstr

A multiscale approach of nonlinear composites under finite deformation: Experimental characterization and numerical modeling

V. Bouchart [c,*], M. Brieu [a], N. Bhatnagar [b], D. Kondo [a]

[a] Laboratoire de Mécanique de Lille (LML), UMR8107 CNRS, Bd. Paul Langevin, 59650 Villeneuve D'Ascq, France
[b] Mech. Eng. Dpt., Indian Institute of Technology, HausKhaz, New Delhi, India
[c] Laboratoire de mécanique Biomécanique Polymère Structures (LaBPS), EA 4632, Ile du Saulcy, 57045 Metz cedex 1, France

ARTICLE INFO

Article history:
Received 13 August 2009
Received in revised form 21 February 2010
Available online 18 March 2010

Keywords:
Hyperelastic materials
Micromechanics
Experimental study
Composites
Damage mechanics

ABSTRACT

The present paper is devoted to the study of the mechanical behavior of an ethylene propylene diene monomer (EPDM) rubber reinforced by polypropylene (PP) particles, revealed as compressible. The hyperlastic behavior of this blend has been characterized under cyclic uni-axial tensile tests. The experimental results show a significant effect of the fraction of (PP) particles (5%, 10%, 25% and 30% by weight) on the macroscopic behavior of the composite. In order to model this behavior, we first develop and implement a micromechanically-based nonlinear model for hyperelastic composites. The approach is based on the second order homogenization method proposed by Ponte Castaneda and Tiberio (2000) and for which suitable energy densities are adopted for the matrix and the inclusions phases, both assumed as compressible. We then proceed to the model verification by comparison with Finite Element simulations on a unit cell. Finally, we propose an extension of the model in order to take into account damage due to voids growth phenomena. The comparison of the multiscale damage model predictions with the experimental data obtained on the EPDM/PP composite indicates a very good agreement.

1. Introduction

The use of EPDM–PP blends has been continuously growing in various industrial domains for several decades. As it is possible to mix ethylene propylene diene monomer (EPDM) and polypropylene (PP) in any ratio, there is theoretically a wide spectrum of materials from elastified PP to EPDM rubber reinforced with thermoplastics. In this study, we focus on the second type of blend that is an EPDM reinforced with particles of PP (a random dispersion of the PP reinforcements in the EPDM matrix is assumed). In order to gain a better understanding of the mechanical behavior of such blends and to provide a physical basis for their modeling, an experimental study was conducted with the particular objective of quantifying the reinforcing effects of polypropylene particles randomly dispersed in the EPDM.

A second part of the study is devoted to the modeling of the behavior of these blends. For this purpose, two different approaches can be followed to predict the behavior of rubber-like reinforced materials under finite deformation. The first approach is phenomenological and provides pure macroscopic models which can be calibrated by using available experimental database. However, it is generally recognized that, especially for arbitrary loading paths, the predictive capabilities of these models remain very limited. A way to overcome these limitations consists in using micromechanics-based approaches which allow to link the macroscopic behavior of the material to its heterogeneous microstructure. In addition to homogenization models for periodic microstructures (see Brieu and Devries (1999), Lahellec et al. (2004)), there are various attempts in the literature devoted to materials with random microstructures. Within these ones, we focus on the recent developments of nonlinear homogenization techniques proposed by Ponte Castaneda (1996) and adapted to hyperelastic composites by Ponte Castaneda and Tiberio (2000).[1] Results of this basic version of the micromechanical model, which assumes a perfect adhesion between the two compressible phases with no damage phenomena, is first compared to experimental data. Based on this comparison, we propose a first evaluation without bias[2] of the micromechanical model by performing Finite Elements computations on unit cell. A complete version of the model is then proposed; it incorporates damage mechanisms due to voids growth in an hyperelastic materials. The resulting full 3D isotropic damage model is obtained by combining the second order homogenization method with standard thermody-

* Corresponding author. Fax: +33 3 20 33 71 53.
E-mail address: bouchart@enim.fr (V. Bouchart).

[1] No attempt is made here to investigate more complex models incorporating for instance fields fluctuations (see Ponte Castañeda, 2002). The main reason is to keep the simplicity of the model in view of the computational aspects.

[2] At the difference of the real material, the same assumptions as in the model are retained.

0020-7683/$ - see front matter © 2010 Elsevier Ltd. All rights reserved.
doi:10.1016/j.ijsolstr.2010.03.012

namic approaches. The predictions of the micro–macro damage model are then shown and compared, for validation purpose, to the experimental data of the EPDM/PP composite.

2. Experimental study

In this section, we first present the different constituents of the studied blends (EPDM reinforced with particles of PP) and we describe how the test specimens are prepared. Then, we will present the experimental protocol used to perform the uni-axial tensile test. These tests are necessary to characterize the mechanical properties of the considered EPDM/PP composites and to study the effect of the fraction of PP on the behavior of the blends.

2.1. Studied materials and test specimens preparation

Blends considered in the present study are constituted of polypropylene (PP) procured from Reliance Ind. Ltd., grade REPOL HO33MG and an EPDM elastomer procured from Du Pont, grade NORDEL 4770R. The investigations are performed on different types of blend systems prepared with different quantities of PP and EPDM: 5%, 10%, 25% and 30% by weight of PP.

The different compositions were made by means of a co-rotating intermeshing twin-screw extruder. The granules of PP and EPDM were mixed in appropriate ratios prior to being added to the extruder hopper. The screw speed was adjusted to 240 rpm while the die zone temperature was maintained at 210 °C; the filament obtained upon extrusion was immediately quenched in water and later chopped into small granules. The specimens for mechanical testing (ASTM D638) were prepared by injection molding using LT Demag PFY40-LNC4P Machine. The nozzle temperature was maintained at 210 °C, and the injection pressure at 60 MPa. Moreover, from SEM micrographs of cryogenically fractured samples of the blends, a more or less uniform dispersion of PP particles in the EPDM matrix is noted.

2.2. Characterization of the mechanical behavior of the blend

2.2.1. Experimental protocol

The mechanical tests have been carried out by using a uni-axial tensile machine (INSTRON 4302) with a low load cell capacity (1 kN). This cell is well adapted to the study of hyperelastic material. In order to avoid the slippage of the samples, mainly due to the quasi incompressible behavior of the involved materials, the grips are self-tightening based on an eccentric system (Fig. 1(b)). Because of the large deformations which occur in elastomeric materials, the measurements of stretch have been performed using a contactless video extensometer at a constant strain rate (10^{-3}/s) (see adapted samples in Fig. 1(a)). Each test has been performed several (5 in average) times in order to guarantee its good reproducibility; thus, only the average data are shown in the present study. In order to characterize the hyperelastic behavior of the EPDM and of the blends, a set of tests is carried out on specimens subjected to uni-axial cyclic loadings with imposed maximal stretch and a zero minimal stress.

2.2.2. Experimental results

Before presenting the macroscopic response of the blends, let us first describe the mechanical behavior of the constituents.

In Fig. 2 is presented the response of the polypropylene (PP) phase; it is observed that the PP phase exhibits a high rigidity while it fails at a relative small strain level (deformation less than 15%).

Let us discuss now the behavior of pure EPDM, that of its blends with PP being discussed henceforth. The obtained results for cyclic loadings are presented in Fig. 3 for the pure EPDM and for the EPDM90–PP10, that is 90% EPDM and 10% PP. One can notice that the rigidity of the composite material increases by blending of PP amorphous phase with EPDM and that the PP phase has a clear reinforcement effect on the EPDM matrix.

In order to characterize the pure hyperelastic behavior of rubber-like materials without taking into account the Mullins damage and viscosity phenomena (see Mnllins (1969), Diani et al. (2006b)), it is usual to consider materials which have been loaded once until the considered maximum of stretch and to focus only on the unloaded part of the response since it presents a low viscosity (see for instance Miehe (1995), Diani et al. (2006a)). For the different blends, this analysis confirms the reinforcement effect of PP on the EPDM (see Fig. 4). As expected, the reinforcing effect increases with the increase of weight of PP phases.

3. Micromechanical model of hyperelastic behavior: formulation and predictions for the reinforced material

In agreement with the specific heterogeneous nature of the studied material, the mechanical behavior is modeled by means

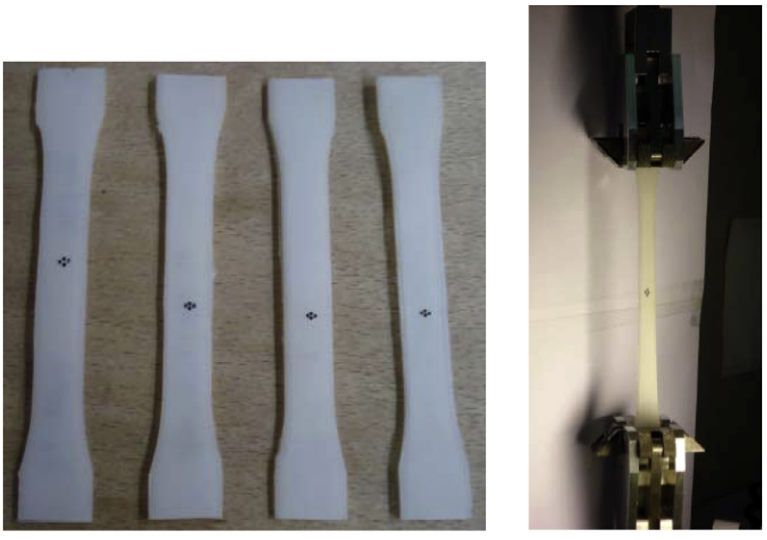

(a) EPDM-PP samples with 4 markers (b) Tested sample

Fig. 1. Tested sample and testing system.

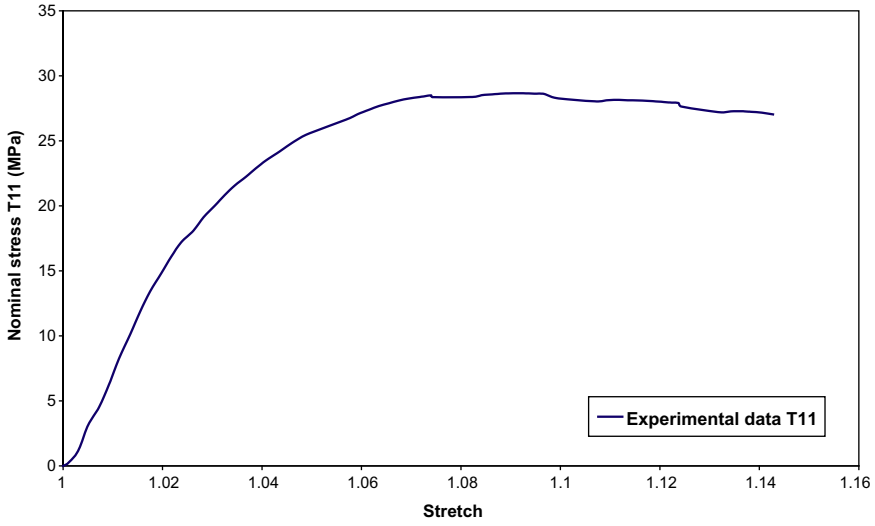

Fig. 2. Experimental response of the PP phase under uni-axial loading.

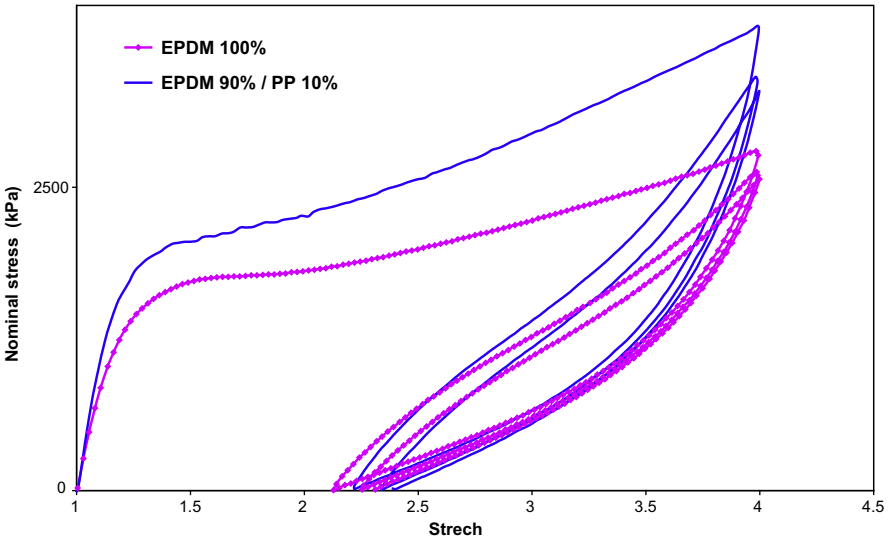

Fig. 3. Mechanical response of the pure EPDM and of the EPDM90–PP10 blend under cyclic uni-axial tensile loading.

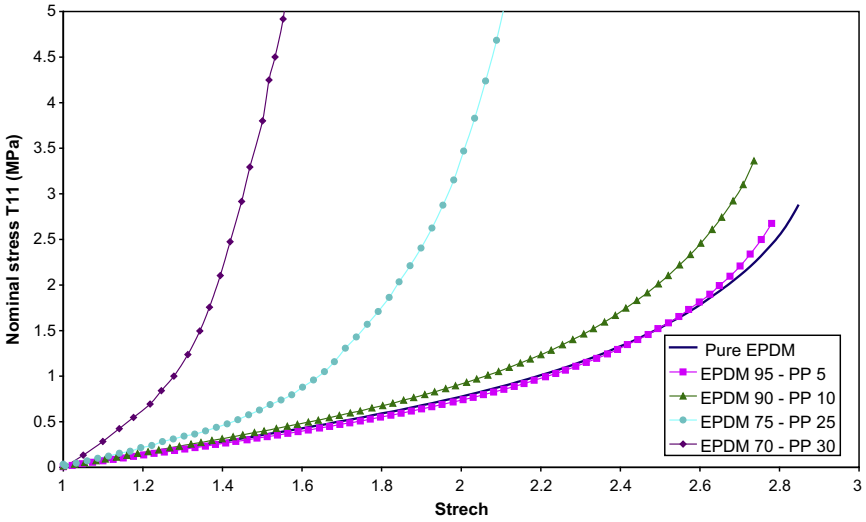

Fig. 4. First unloading of the pure EPDM and of different blends EPDM–PP.

of a nonlinear homogenization method devoted to materials with random microstructure.

3.1. Basic principles and equations of the second order method

From the modelling point of view, the PP amorphous phase is considered as reinforcing particles in EPDM matrix, as it has been noticed on SEM observations.

Let us consider a representative elementary volume (REV), denoted Ω_0, and composed of an hyperelastic matrix reinforced by a random distribution of particles. This REV is assumed to occupy a volume V_0 in the reference configuration and to satisfy the standard scale separation conditions. This heterogeneous material is subjected to homogeneous boundary strain conditions: $\underline{u} = (\overline{\mathbf{F}} - \mathbf{I}) \cdot \underline{X}$ on $\partial\Omega_0$. The heterogeneous deformation gradient tensor $\mathbf{F}$ satisfies then $\overline{\mathbf{F}} = \langle \mathbf{F} \rangle$ with $\langle . \rangle$ the volume average over Ω_0.

It is assumed here that in the REV, the dispersed PP particles and the EPDM matrix obey to hyperelastic constitutive laws which are determined by their strain energy densities $W^{(r)}(\mathbf{F})$[3] (r=1,...,N). We make use now of a fundamental result by Hill (1972): the homogenized constitutive law, giving the macroscopic first Piola–Kirchoff stress tensor $\overline{\mathbf{T}} = \langle \mathbf{T} \rangle$, is determined by a macroscopic strain energy density $\widetilde{W}$ such that:

$$\overline{\mathbf{T}}(\overline{\mathbf{F}}) = \frac{\partial \widetilde{W}(\overline{\mathbf{F}})}{\partial \overline{\mathbf{F}}} \tag{1}$$

In order to assess the macroscopic energy of nonlinear heterogeneous materials, various approaches can be considered (see Ponte Castañeda and Suquet (1998)). Among these approaches, mention can be made of the second order homogenization method, introduced by Ponte Castaneda (1996). This method is based on a linearization of the strain energy densities of each phase, $W^{(r)}(\mathbf{F})$, by using a Taylor expansion and then introducing a linear comparison composite. It appears to be particularly accurate and its extension to finite deformation has been performed by Ponte Castaneda and Tiberio (2000). Let us then denote by "1" the hyperelastic matrix containing a unique population of spherical particles, denoted by "2". For this two-phase hyperelastic composite, the second order method can be particularized and provides the following estimate of the macroscopic strain energy density:

$$\widetilde{W}(\overline{\mathbf{F}}) \simeq \sum_{r=1}^{2} c^{(r)} \left\{ W^{(r)}(\overline{\mathbf{F}}^{(r)}) + \frac{1}{2} (\overline{\mathbf{F}} - \overline{\mathbf{F}}^{(r)}) : \mathbf{T}^{(r)}(\overline{\mathbf{F}}^{(r)}) \right\} \tag{2}$$

where $\mathbf{T}^{(r)}(\overline{\mathbf{F}}^{(r)}) = \frac{\partial W^{(r)}}{\partial \mathbf{F}}(\overline{\mathbf{F}}^{(r)})$ and $c^{(r)}$ is the volume fraction of phase r.

The macroscopic, stress tensor, given by the derivative of (2) with respect to $\overline{\mathbf{F}}$, is then estimated by:

$$\overline{\mathbf{T}}(\overline{\mathbf{F}}) \simeq \sum_{r=1}^{2} \frac{c^{(r)}}{2} \left[\mathbf{T}^{(r)}(\overline{\mathbf{F}}^{(r)}) + [\mathbf{T}^{(r)}(\overline{\mathbf{F}}^{(r)}) + \mathbb{L}^{r}(\overline{\mathbf{F}}^{(r)}) : (\overline{\mathbf{F}} - \overline{\mathbf{F}}^{(r)})] : \frac{\partial \overline{\mathbf{F}}^{(r)}}{\partial \overline{\mathbf{F}}} \right] \tag{3}$$

where $\mathbb{L}^{r}(\overline{\mathbf{F}}^{(r)}) = \mathbb{L}_{t}^{r}(\overline{\mathbf{F}}^{(r)}) = \frac{\partial^2 W^{(r)}}{\partial \mathbf{F} \partial \mathbf{F}}(\overline{\mathbf{F}}^{(r)})$.

This leads, by average rule on the REV, to the following expression for the average stresses, $\mathbf{S}^{(r)}$, in each phase r:

$$\mathbf{S}^{(r)}(\overline{\mathbf{F}}) \simeq \frac{1}{2} \left[\mathbf{T}^{(r)}(\overline{\mathbf{F}}^{(r)}) + [\mathbf{T}^{(r)}(\overline{\mathbf{F}}^{(r)}) + \mathbb{L}^{r}(\overline{\mathbf{F}}^{(r)}) : (\overline{\mathbf{F}} - \overline{\mathbf{F}}^{(r)})] : \frac{\partial \overline{\mathbf{F}}^{(r)}}{\partial \overline{\mathbf{F}}} \right] \tag{4}$$

Obviously, this expression is derived from the theoretical homogenization framework proposed by Ponte Castaneda and Tiberio (2000). Note that, more elaborated expressions are available when local field fluctuations are taken into account as in Idiart and Ponte Castañeda (2007).

[3] The superscript (r) stands for a constituent r.

Note that the only unknowns in (3) and (4) are the average deformation gradients in each phase r, $\overline{\mathbf{F}}^{(r)}$, which may be computed from the resolution of a fictitious thermoelastic problem related to the linear comparison composite involved in the method. In the case of two-phase materials, the resolution of this thermoelastic problem is performed according to the Levin's theorem Levin (1967) which reads:

$$\overline{\mathbf{F}}^{(r)} = \mathbb{A}^{(r)}(\overline{\mathbf{F}}^{(r)}) : \overline{\mathbf{F}} + \left(\mathbb{A}^{(r)}(\overline{\mathbf{F}}^{(r)}) - \mathbb{I} \right) : (\Delta \mathbb{L})^{-1} : (\Delta \boldsymbol{\tau}); \quad r = 1, 2. \tag{5}$$

where $\Delta \mathbb{L} = \mathbb{L}^{(1)}(\overline{\mathbf{F}}^{(1)}) - \mathbb{L}^{(2)}(\overline{\mathbf{F}}^{(2)})$, $\Delta \tau = \boldsymbol{\tau}^{(1)}(\overline{\mathbf{F}}^{(1)}) - \boldsymbol{\tau}^{(2)}(\overline{\mathbf{F}}^{(2)})$.

$\boldsymbol{\tau}^{(r)} = \mathbf{T}^{(r)}(\overline{\mathbf{F}}^{(r)}) - \mathbb{L}^{r} : \overline{\mathbf{F}}^{(r)}$ represents polarization tensors which can be seen as fictitious thermal stress tensors and $\mathbb{A}^{(r)}$ is the localization tensor associated to phase (r) in the linear comparison composite. $\mathbb{A}^{(r)}$ depends on the linear homogenization scheme used to solve (5). In the present study, the matrix-inclusion type morphology of the (reinforced) material suggests to consider the well-known Hashin–Shtrikman bound (see Hashin and Shtrikman (1962)). This bound which allows in particular to account for the interactions between the different constituents is characterized by the following expression of the localisation tensors:

$$\mathbb{A}^{(1)} = \left[c^{(1)} \mathbb{I} + c^{(2)} [\mathbb{I} - \mathbb{P} : \Delta \mathbb{L}]^{-1} \right]^{-1}; \quad \mathbb{A}^{(2)} = \left[\mathbb{I} - c^{(1)} \mathbb{P} : \Delta \mathbb{L} \right]^{-1} \tag{6}$$

in which $\mathbb{I}$ is the fourth order unit tensor. The micromechanical model, considered in the following, will be then referred as HS-based model.

3.2. Numerical implementation

The implementation of the considered homogenization model requires the use of suitable numerical methods, among others, to compute the Hill tensor $\mathbb{P}$ in the HS-based model, the tangent modulus tensor of each phase $\mathbb{L}^{(r)}$ being anisotropic. Thus, recalling that the spherical particles are randomly dispersed in the matrix, so that the composite remains statistically isotropic in the undeformed configuration, the Hill tensor reads (see Willis (1977)):

$$\mathbb{P} = \frac{1}{4\pi} \int_{|\xi|=1} \mathbb{H}^{(1)}(\xi) dS. \tag{7}$$

where $\mathbb{H}_{ijkl}^{(1)}(\xi) = \mathbf{N}_{ik}^{(1)} \xi_j \xi_l$, $\mathbf{N}^{(1)} = \mathbf{K}^{(1)^{-1}}$, $\mathbf{K}_{ik}^{(1)} = \mathbb{L}_{ijkl}^{(1)} \xi_j \xi_l$.

A Gaussian integration technique has been implemented for the numerical integration over the surface of the unit sphere, $|\xi| = 1$.

Numerical techniques are also needed to solve the system of nonlinear equations (5) associated to the fictitious thermoelasticity problem. For this resolution, one must determine $\overline{\mathbf{F}}^{(1)}$ and $\overline{\mathbf{F}}^{(2)}$, for instance by using the Newton–Raphson method. Note that the Jacobian matrix, $\mathbf{J}$, introduced in that method, is in the present case a 9×9 matrix.

Due to the lack of a closed-form expression for $\mathbb{P}$, the Jacobian matrix can not be analytically expressed. Consequently, a numerical derivation by finite difference was also used. In order to get a good accuracy, an iterative scheme, namely the Ridders–Richardson method was implemented. This method is based on an algorithm in which a control and optimization of the numerical errors are performed at each step of the procedure. Further details on this numerical procedure may be found in Press et al. (1992).

Once the resolution of the problem is achieved for the two phase material, it is possible to compute the macroscopic stress tensor from (3). To this end, it is necessary to perform the numerical derivation of $\overline{\mathbf{F}}^{(1)}$ and $\overline{\mathbf{F}}^{(2)}$ with respect to $\overline{\mathbf{F}}$.

3.3. Application to the EPDM/PP blends

We present here the application of the HS-based model for the EPDM/PP blend in the case of a monotonous uni-axial tensile load-

ing. Due to compressibility of each material phases, for this loading, the associated macroscopic deformation gradient is written in the form: $\overline{\mathbf{F}} = \mathrm{Diag}(\lambda, \alpha, \alpha)$, λ increasing from 1.0.

Because of the deformation-based control of the uni-axial tensile loading applied to the composite, for a given λ, one has to determine the value of α which fulfills the uni-axial tensile condition: $\overline{\mathbf{T}} = \mathrm{Diag}(T_{11}, 0, 0)$.

For more details concerning the implementation of the method in this case, the readers may refer to Bouchart et al. (2008) and Bouchart (2007).

In order to apply the homogenization method to the studied composite, we need to choose suitable strain energy densities to model the behavior of the matrix phase and of the inclusion one. Thus, for the compressible EPDM matrix, the density introduced by Lambert-Diani and Rey (1999) is adopted. According to these authors, this density (see (8)) is adequate for the modeling of elastomers deformation even for high elongation. Due to the very low rigidity of the EPDM, the PP phase is considered to be subjected to infinitesimal strain. Accordingly, the behavior of particles is described by the strain energy density proposed by Ciarlet and Geymonat (1982).

Each constituent of the composite being isotropic, the strain energy density $W^{(1)}$ and $W^{(2)}$ are expressed as functions of the three invariants, I_1, I_2 and I_3 of the dilatation tensor $\mathbf{C}={}^t\mathbf{F}\mathbf{F}$ (see for instance Ogden (1984)). In particular, the Diani–Lambert and Rey's density reads:

$$\mathrm{W}^{(1)}(\mathbf{F}) = \int_3^{I_1} e^{\left(\alpha_0+\alpha_1(I_1-3)+\alpha_2(I_1-3)^2\right)} dI_1 + \int_3^{I_2} \beta_1 I_2^{\beta_2} dI_2 \tag{8}$$

where α_0, α_1, α_2, β_1, β_2 are the model parameters for the matrix phase which have to be identified on experimental data for the considered EPDM.

For the PP phase, the energy density proposed by Ciarlet and Geymonat is adopted:

$$\mathrm{W}^{(2)}(\mathbf{F}) = C_1(I_1-3) + C_2(I_2-3) + C_3(I_3-1) - B\ln(I_3) \tag{9}$$

where C_1, C_2, C_3 and B are model parameters which have also to be identified.

Even if, in the present work, strain energy density is sometimes depending on the two first invariants of the Cauchy–Green strain tensor only, the considered behavior is compressible. Indeed, any hydrostatic pressure is introduced and stresses in each phases are defined by $\mathbf{T}^{(r)}(\overline{\mathbf{F}}^{(r)}) = \frac{\partial \mathrm{W}^{(r)}}{\partial \mathbf{F}}(\overline{\mathbf{F}}^{(r)})$.

Let us present now the principle of the identification. For a uni-axial tensile loading (TU), $\mathbf{F} = Diag(\lambda, \alpha, \alpha)$ (α being determined in order to fulfill the uni-axial tensile condition), the expressions of the principal invariants and the nominal stresses (Piola–Kirchhoff 1) are:

$$\begin{cases} I_1 = \lambda^2 + 2\alpha^2 \\ I_2 = \alpha^2(\alpha^2 + 2\lambda^2) \\ I_3 = \lambda^2\alpha^4 \\ T_{11}^{TU-theoretical} = 2\lambda\left[\frac{\partial \mathrm{W}}{\partial I_1} + 2\frac{\partial \mathrm{W}}{\partial I_2}\alpha^2 + \frac{\partial \mathrm{W}}{\partial I_3}\alpha^4\right] \\ T_{22}^{TU-theoretical} = T_{33}^{TU-theoretical} = 2\alpha\left[\frac{\partial \mathrm{W}}{\partial I_1} + \frac{\partial \mathrm{W}}{\partial I_2}(\lambda^2+\alpha^2) + \frac{\partial \mathrm{W}}{\partial I_3}\lambda^2\alpha^2\right] \end{cases} \tag{10}$$

To identify the parameters of a strain energy density from uni-axial tensile tests results, the following conditions have to be fulfilled:

$$\begin{cases} \text{(i)} T_{11}^{TU-experimental} = T_{11}^{TU-theoretical} \\ \text{(ii)} T_{22}^{TU-theoretical} = T_{33}^{TU-theoretical} = 0 \\ \text{(iii)} T_{ij}^{TU-theoretical}(\mathbf{F}) = 0 \quad (i,j = 1\ldots3) \text{ when } \mathbf{F} = \mathbf{I} \end{cases} \tag{11}$$

The determination of parameters has been done by the method of least squares, minimizing the relative error in stresses, denoted E_{rror}, by simultaneous verification of the conditions (i), (ii), (iii). For the n stress/strain pairs, the relative error measured, E_{rror}, can be given as:

$$E_{rror} = \sum_{i=1}^{n}\left(1 - \frac{theoretical\ stress}{experimental\ stress}\right)^2$$

The results of the identification procedure are presented in Fig. 5(a) for the pure EPDM and in Fig. 5(b) for the PP, until 6% of deformation. The following values of the parameters are obtained for the EPDM:

$$e^{\alpha_0} = 0.2246\ \text{MPa}; \quad \alpha_1 = 0.013051; \quad \alpha_2 = 0.024$$
$$e^{\beta_1} = 0.38104\ \text{MPa}; \quad \beta_2 = -2.03234.$$

and for the PP phase:

$$C_1 = -827\ \text{MPa}; \quad C_2 = 963\ \text{MPa}; \quad C_3 = 100\ \text{MPa}; \quad \text{and}$$
$$B = 1199\ \text{MPa}$$

It is desirable to determine elastic properties corresponding to these values. To this end, we determine the Cauchy stresses from the Piola–Kirchhoff 1 ones $\mathbf{T} = \frac{\partial \mathrm{W}(\mathbf{F})}{\partial \mathbf{F}}$; for example, the obtained expression for the Lambert–Diani and Rey's density is:

$$\boldsymbol{\sigma} = \frac{1}{J}\mathbf{T}\mathbf{F}^t = \frac{2}{J}\left(e^{\left(\alpha_0+\alpha_1(I_1-3)+\alpha_2(I_1-3)^2\right)} + \beta_1 I_2^{\beta_2} I_1\right)\mathbf{B} - \frac{2}{J}\beta_1 I_2^{\beta_2}\mathbf{B}.\mathbf{B} \tag{12}$$

where $\mathbf{B} = \mathbf{F}\mathbf{F}^t$ is the left strain tensor of Cauchy-Green.

After linearization, this leads, at infinitesimal deformation, to Lame coefficients: $\lambda = 2e^{\alpha_0}(2\alpha_1 - 1) + \frac{16}{3}\beta_1\beta_2 3^{\beta_2} = 0.7$ MPa and $\mu = 2(e^{\alpha_0} + \beta_1 3^{\beta_2}) = 0.24$ MPa, for the matrix. Thus, the Young modulus is $E = 0.7$ MPa and the Poisson ratio $\nu = 0.37$. For the particles, the same approach can be followed for the Ciarlet–Geymonat density and one obtains, after linearization, $E = 800$ MPa and $\nu = 0.47$. One may note that the experimental characterization of the matrix and the reinforcement has revealed a compressible behavior of each phase. This confirms the compressibility assumption already adopted for the micromechanical modeling. Such behavior may found its origin in the process, injection molding, used to elaborate the composite. The same process has also been used to produce the pure matrix samples in order to avoid bias induced by the process.

Once the identification of strain energy densities for each phase of the studied blends are done, we applied the nonlinear homogenization model whose predictions are presented in Figs. 6 and 7 for the EPDM matrix containing 5% and 10% of PP particles, respectively. It may be noticed that the model give results that are not completely in quantitative agreement with experimental results. This observation first motivated us for rigorous verification of the model, as presented in the following (Section 4).

Note: To apply the homogenization model, we have to transform the weight ratio (c_m) of each constituent into volume ratio (c_v) considered the model. To this end, we have the density of the considered EPDM and PP: $\rho_{EPDM} = 870\ \text{kg/m}^3$ and $\rho_{PP} = 910\ \text{kg/m}^3$, and the following expression gives the composite density:

$$c_{v\,\mathrm{PP}} = \frac{c_{m\,\mathrm{PP}}\,\rho_{\mathrm{EPDM}}}{c_{m\,\mathrm{PP}}\,\rho_{\mathrm{EPDM}} + c_{m\,\mathrm{EPDM}}\,\rho_{\mathrm{PP}}}.$$

To highlight the compressible character of the matrix phase, we illustrate the variation of the third invariant of the local Cauchy–Green tensor, I_3, as a function of the macroscopic strain (see Fig. 8).

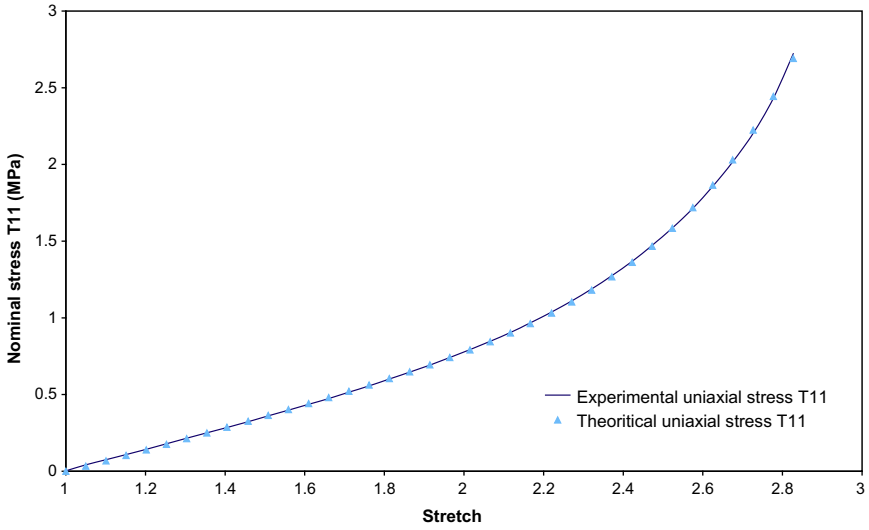

(a) Lambert-Diani and Rey density for the EPDM

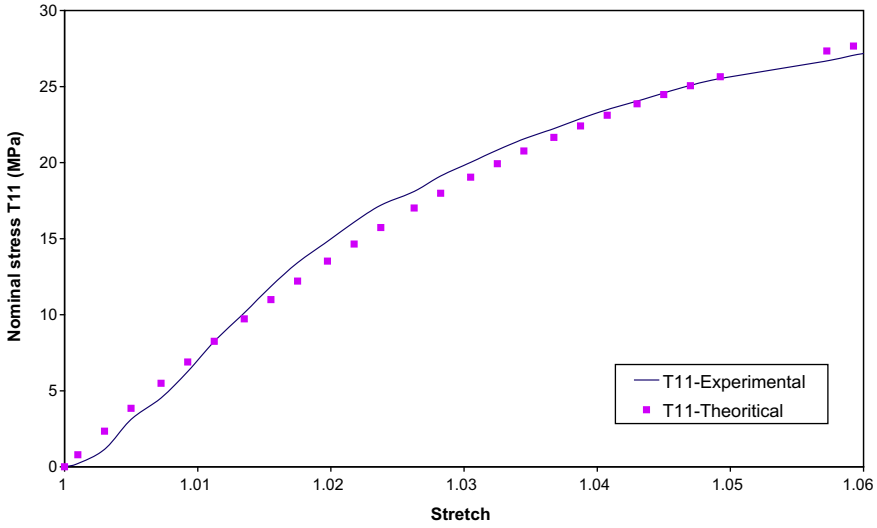

(b) Ciarlet and Geymonat density for the PP particles

Fig. 5. Result of the identification of the densities for each phase.

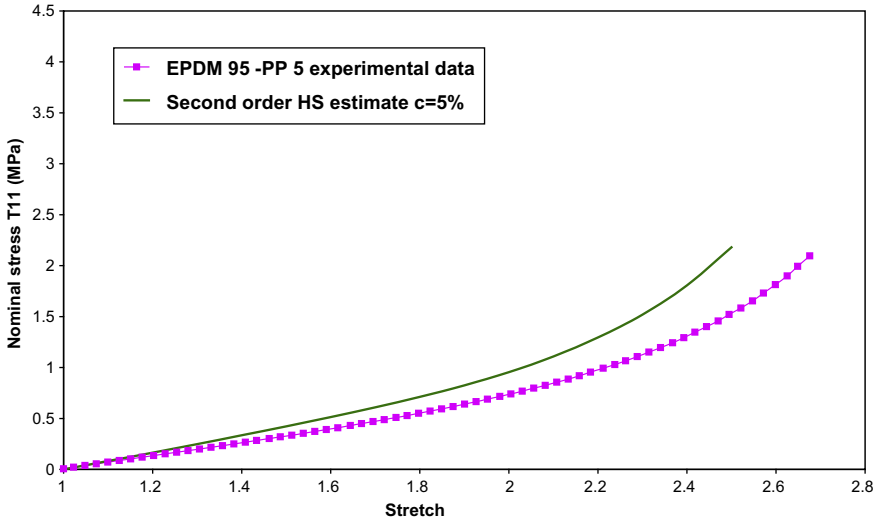

Fig. 6. HS-based model predictions compared to the experimental data for the EPDM with 5% of PP phase.

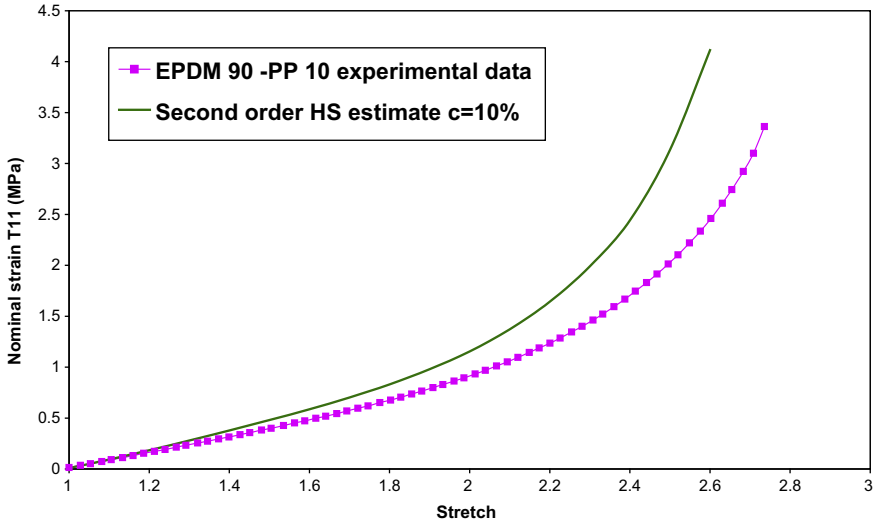

Fig. 7. HS-based model predictions compared to the experimental data for the EPDM with 10% of PP phase.

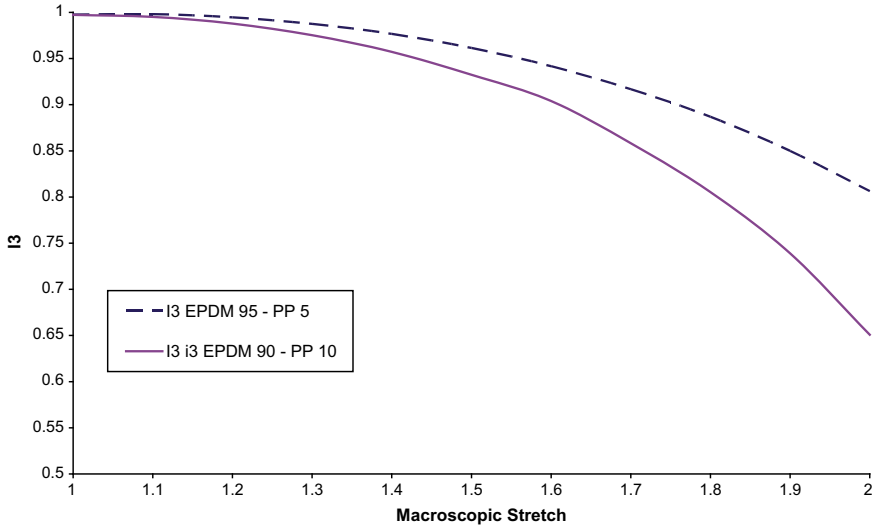

Fig. 8. Variation of I_3 for the EPDM with 5% and 10% of PP phase.

4. Numerical verification by Finite Elements (FE) simulations

4.1. Principle of the FE simulations with hyperelastic model

In order to provide a verification of the model based on the second order method, we follow here the approach described by Bouchart et al. (2008) and in which use has been done of very simple energy densities. The main difference in the work performed and summarized in this section is to provide the same analysis by considering a more realistic energy density adapted for each phase, as presented in Section 3. The objective however is still to carry out a verification of the nonlinear homogenization model by comparing its predictions to reference solutions obtained by Finite Elements (FE) computations. To this end, we consider the same local constitutive law in both homogenization and FE simulations for each material phase.

The FE reference solutions are obtained by considering a cylindrical unit cell which represents the composite material. As illustrated in Fig. 9, the space is supposed to be filled by prisms with hexagonal bases which represent the matrix, each prism contains a spherical particle in its center. This procedure is similar to the one already followed by various authors for elasto-plastic composites materials (see for instance Llorca and Segurado (2004)). That allows one to consider different types of inclusions (rigid or deformable ones but also cavities), considering for each case the suitable parameters in the strain energy density used to describe their behavior.

To take advantage of the symmetry, the 3D unit cells are approximated by cylinders with circular basis to allow axisymmetric computations. Thus, the displacement boundary conditions considered for the simulation of a uni-axial tensile test can be expressed as following:

- $U_z(y,0) = 0,\ 0 < y < R$
- $U_z(y,L) = U_{zimposed},\ 0 < y < R$
- $U_y(0,z) = 0,\ 0 < z < L$
- $U_y(R,z) =$ constant, $0 < z < L$

The last condition yields the same radial displacement for points at the lateral boundary; the value of this displacement is ob-

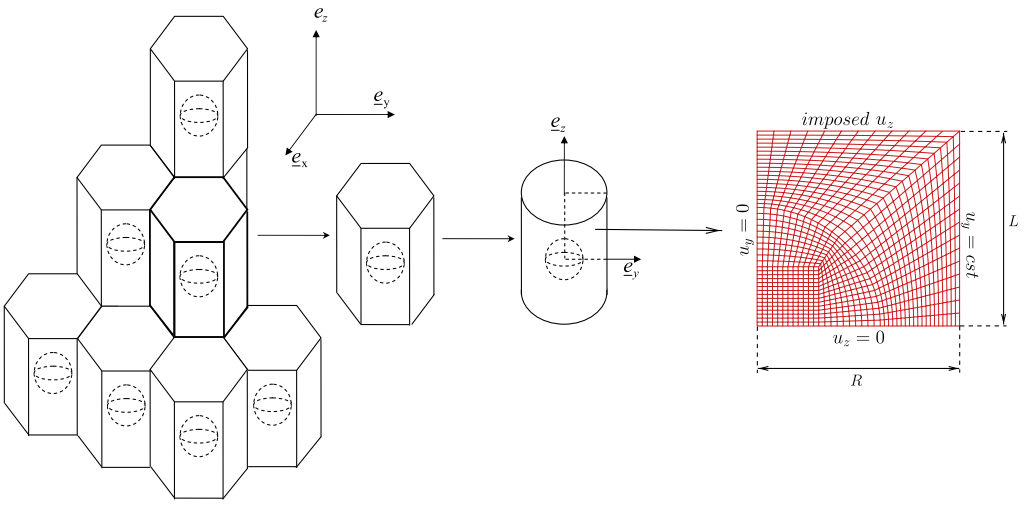

Fig. 9. A periodic network of hexagons with pores; reduction to a 2D axisymmetric unit cell.

tained as the result of the Finite Element computation. The displacement at the top side U_z is prescribed gradually to reach the required strain at the end of the simulation.

The FE simulations were performed using the commercial software Abaqus; the unit cell used contains CAX8R elements (8-node biquadratic axisymmetric quadrilaterals, with reduced integration). These FE simulations provide heterogeneous strain and stress fields in the unit cell from which their volume average can be computed by using a specific post-treatment script.

Since the energy densities used are not available in the Abaqus software, we have first proceeded to their implementation in this software via the user routine UMAT. To do this, we have programmed, in FORTRAN, a subroutine specific to the model corresponding to the considered density. A number of entries of this subroutine are managed by Abaqus, but the user must provide the components of the Cauchy stress tensor and the Jacobian matrix of this stress with respect to the nominal strain for a given current value of the strain. The Abaqus software works in updated Lagrangian, at the end of each increment, the values of state variables of the model must be updated to observe continuous change.

Let us recall that the Cauchy stresses are given by (12) for the Lambert–Diani and Rey's density and that the same type of expression can be found for the Ciarlet–Geymonat one.

Thus, Jacobian matrix $\mathbb{C}$ of the corresponding material is defined by the variation of the stresses $J\boldsymbol{\sigma}$:

$$\delta(J\boldsymbol{\sigma}) = J\mathbb{C} : \delta\mathbf{D} \tag{13}$$

where $\delta\mathbf{D}$ is the virtual deformation rate which is the symmetric part of the gradient of displacement variation. In fact, it is possible to express all of the quantities in $\delta(J\boldsymbol{\sigma})$ depending on $\delta\mathbf{D}$ (for more details, see the Abaqus manual (ABAQUS, 2004)). This allows to determine the Jacobian matrix of the material (see Appendix A).

4.2. Comparisons of model predictions with FE simulations

For the purpose of comparison, a volume fraction of particles equal to 10% is considered. The comparison between the predicted macroscopic behavior and the results computed from the FE solution, shown in Fig. 10(a), indicates a good agreement which is confirmed by the comparison of the local average stress in the matrix phase (see Fig. 10(b)).

It is also interesting to investigate the strain field induced in the composite material by the macroscopic tensile loading (see Fig. 11(a)). Although a significant heterogeneity of the strain is observed, it appears that the homogenization method provides a very accurate estimate of the average deformation in the solid matrix phase (see comparison in Fig. 11(b)).

Thus, recalling that the homogenization model was not in good agreement with experimental data, and taking into account its verification by means of Finite Element simulations, we came to the conclusion that it is necessary to include other mechanisms of deformation in the model. In the following section, the aim will be to take into account the damage phenomena which may occur in elastomeric materials during the loading. Specifically, we explore the modeling of the presence and/or growth of microcavities in the nonlinear hyperelastic matrix. This porosity may already exist in the material before mechanical loading (e.g. due to the manufacturing process) or induced at the matrix–particles interface during the loading. Indeed, it is convenient to recall that the studied composite does not contain any compatibilizer; the particles–matrix adherence may not be perfect.

5. Incorporation of damage in the micromechanical hyperelastic model

It is commonly recognized that defects and voids significantly affect the macroscopic response of hyperelastic materials. Various attempts have been done in the past and continue for the mechanical modeling of this class of voided hyperelasic materials. Blatz and Ko (1962) proposed a phenomenological approach of porous elastomers which has been recently applied to the analysis of fracture growth by Kakavas (2002). However, the phenomenological formulation of these models still limits their domain of applicability. In the framework of continuum micromechanics, mention can be made of the study by Govindgee and Simo (1991) and more recently by Danielsson et al. (2004) who consider a kinematically admissible deformation field in order to evaluate the macroscopic density of the porous material. As already pointed out by Lopez-Pamies and Ponte Castañeda (2007), the model proposed by Danielsson et al. (2004) corresponds rigorously to an upper bound for *composite sphere assemblage* microstructure of Hashin. The second order homogenization method provides a more suitable model which can be applied to more general microstructures.

The principal objective of the present section is to derive a damage model based on the second order homogenization method applied in the above sections to hyperelastic porous materials. Before that, we will present the second order method adapted for porous

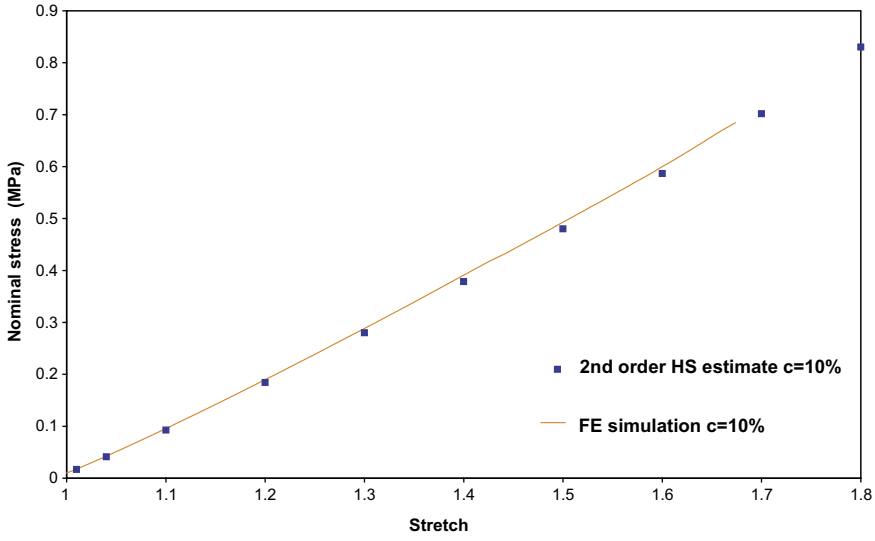

(a) Macroscopic response under uni-axial tensile loading

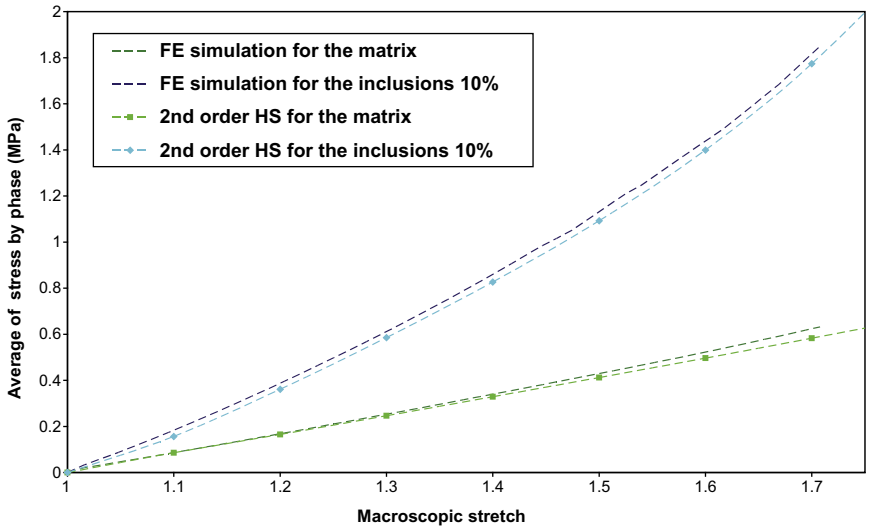

(b) Local longitudinal strain average in each phase

Fig. 10. HS-based model predictions compared to the numerical response for the hyperelastic material with 10% of PP spherical particles.

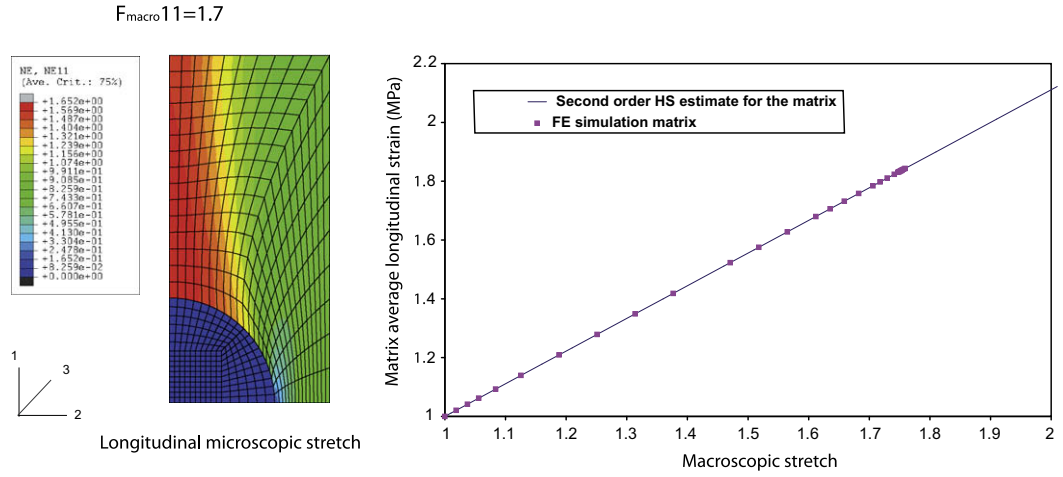

(a) Longitudinal strain field (b) Average longitudinal strain in the matrix phase

Fig. 11. Predictions of HS-based model compared to the numerical response for the EPDM with 10% of PP.

hyperelastic materials and will check its validity. For this, a comparison with FE simulations will be also performed.

5.1. The second order homogenization method for 3D hyperelastic porous materials

The adaptation of the second order homogenization method to porous hyperelastic material can be easily performed by modeling the microcavities as hyperelastic media with a strain energy density $W^{(2)}$ equal to zero. Thus, the estimate of the macroscopic strain energy density $\widetilde{W}$ for the porous material can be read as:

$$\widetilde{W}(\overline{\mathbf{F}}) \simeq (1-c)\left\{W^{(1)}(\overline{\mathbf{F}}^{(1)}) + \frac{1}{2}(\overline{\mathbf{F}} - \overline{\mathbf{F}}^{(1)}) : \mathbf{T}^{(1)}(\overline{\mathbf{F}}^{(1)})\right\} \tag{14}$$

with $\overline{\mathbf{F}}^{(r)}$ given by (5) which reduces to:

$$\overline{\mathbf{F}}^{(r)} = \mathbb{A}^{(r)}(\overline{\mathbf{F}}^{(r)}) : \overline{\mathbf{F}} + \left(\mathbb{A}^{(r)}(\overline{\mathbf{F}}^{(r)}) - \mathbb{I}\right) : \left(\mathbb{L}^{(1)}(\overline{\mathbf{F}}^{(1)})\right)^{-1} : \boldsymbol{\tau}^{(1)}(\overline{\mathbf{F}}^{(1)}); \quad r = 1, 2. \tag{15}$$

Note: For the Hashin–Shtrikman bound, due to the dependence of the localization tensors (6) (and therefore of $\overline{\mathbf{F}}^{(1)}$) with c, expression (14) of the macroscopic strain energy density may depend nonlinearly on c. Comparatively, the Voigt bound (model by Govindgee and Simo (1991), which corresponds to an assumption of uniform strain in the material ($\overline{\mathbf{F}}^{(1)} = \overline{\mathbf{F}}^{(2)} = \overline{\mathbf{F}}$), provides the following estimate, $\widetilde{W}(\overline{\mathbf{F}}) \simeq (1-c)W^{(1)}(\overline{\mathbf{F}})$, linear with c. Note also that this first order bound leads to an incompressible behavior for the porous material when the matrix is itself incompressible; this in fact not in agreement with the physical expectation of compressibility due to the porosity.

For the implementation of the nonlinear micromechanical HS-based model for porous materials, the method is in the same way as the one which was presented in Section 3.2.

5.2. Numerical verification by Finite Elements simulations

The aim here is to verify the predictions of the second order homogenization method by comparison with Finite Element results in the case of porous hyperelastic material. The FE simulations are performed in the same way as described in Section 4 which allows to considerer spherical cavities and to model their deformation by means of a strain energy density $W^{(2)}$ equal to zero. The considered matrix is still the EPDM elastomer which is modeled again with the strain energy density (8) and the same parameters as before. The spherical voids are modeled by using a strain energy density available in the Abaqus software with suitable values of parameters:

$$W^{(2)}(\mathbf{F}) = C_{10}(J^{-2/3}I_1 - 3) + \frac{1}{D_1}(J-1)^2 \tag{16}$$

where $J = \sqrt{I_3}$ and the model parameters are taken as $C_{10} \to 0$ and $D_1 \to \infty$. In practice, we have considered $C_{10} = 10^{-5}$ MPa and $D_1 = 10^4$ MPa^{-1}.

For the purpose of comparison, a porosity of 15% is considered. The comparison between the predicted macroscopic behavior and the results computed from the FE solution is shown in Fig. 12 and indicates a good agreement. It is also interesting to investigate the strain field induced in the porous material by the tensile loading (see Fig. 13(a)). Although a significant heterogeneity of the strain is observed, as in the unvoided composite, it appears that the homogenization method provides a very accurate estimate of the average deformation in the solid matrix phase (see comparison in Fig. 13(b)).

5.3. Description of the micromechanics-based damage model

In the perspective of evolving damage modeling, we consider now a porosity and develop a micromechanical approach based on expression (14) of the macroscopic density corresponding to porous hyperelastic material. This density will play the role of a thermodynamical potential of the damaged material, in which the porosity c can be considered as the internal damage variable. $\overline{\mathbf{F}}$ and c are the state variables. Obviously, it comes that, in contrast to purely macroscopic approaches, the homogenization method provides not only a clear physical imeaning of the damage variable, but also gives us the expression of $\widetilde{W}$, that is the way the damage affects the material behavior. As already stated, this expression strongly depends on the homogenization scheme used for the resolution of (15).

As classically, the first state law, derived from $\widetilde{W}$, reads similarly to (3) as:

$$\overline{\mathbf{T}}(\overline{\mathbf{F}}, c) = \frac{\partial \widetilde{W}(\overline{\mathbf{F}}, c)}{\partial \overline{\mathbf{F}}}.$$

The thermodynamical force, $\mathscr{F}$, associated to the damage variable c, is given by the second state law:

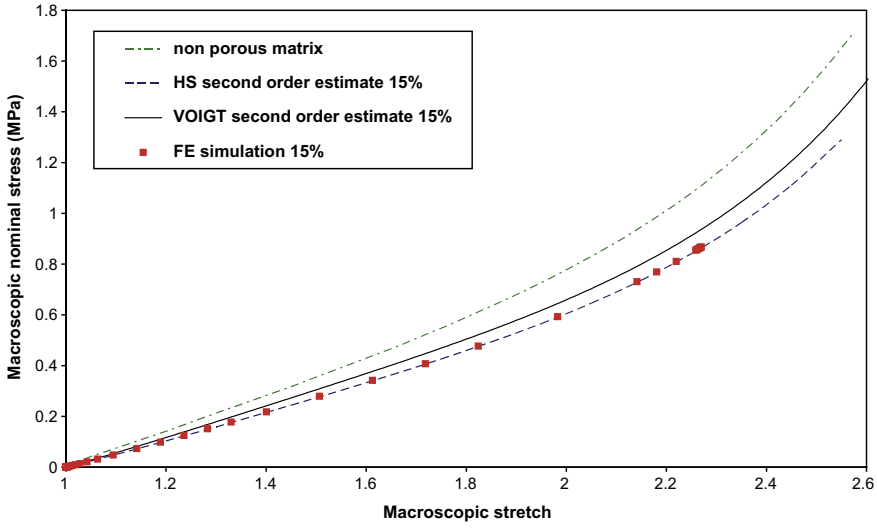

Fig. 12. HS-based model predictions compared to the numerical response for the hyperelastic material with 15% of porosity: macroscopic response under uni-axial tensile loading.

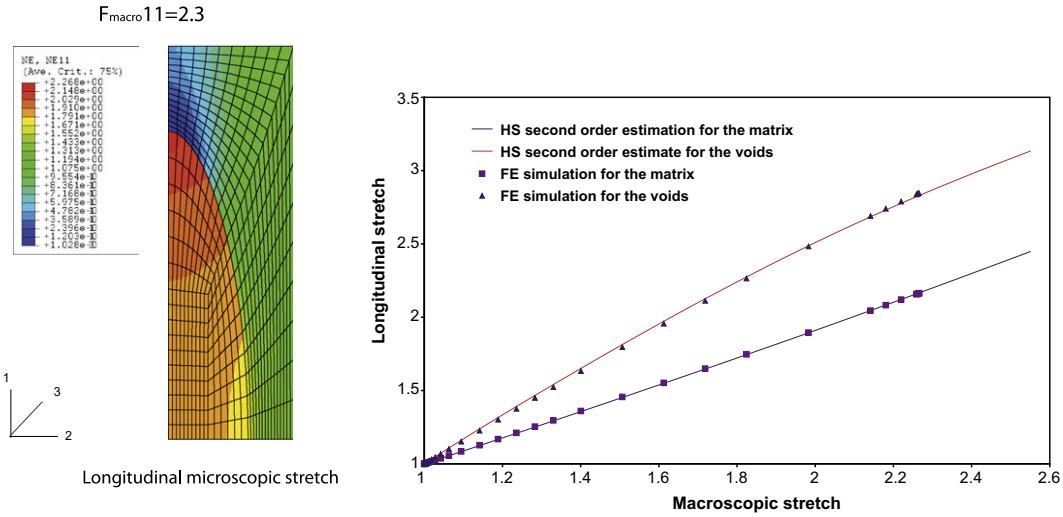

(a) Longitudinal strain field (b) Average longitudinal strain in each phase

Fig. 13. Predictions of the HS-based model compared to the numerical response (15% of porosity).

$$\mathscr{F} = -\frac{\partial \widetilde{W}(\overline{\mathbf{F}}, c)}{\partial c} \tag{17}$$

$$\mathscr{F} = W^{(1)}(\overline{\mathbf{F}}^{(1)}) + \frac{1}{2}(\overline{\mathbf{F}} - \overline{\mathbf{F}}^{(1)}) : \mathbf{T}^{(1)}(\overline{\mathbf{F}}^{(1)}) - \frac{(1-c)}{2}\left[\mathbf{T}^{(1)}(\overline{\mathbf{F}}^{(1)}) + (\overline{\mathbf{F}} - \overline{\mathbf{F}}^{(1)}) : \mathbb{L}^{1}(\overline{\mathbf{F}}^{(1)})\right] : \frac{\partial \overline{\mathbf{F}}^{(1)}}{\partial c} \tag{18}$$

Although, the Hashin–Shtrikman bound is the principal homogenization scheme used in the study, it is interesting to point out that for the Voigt scheme, the macroscopic stress, $\overline{\mathbf{T}}(\overline{\mathbf{F}}, c) = (1-c)\,\mathbf{T}^{(1)}(\overline{\mathbf{F}})$, depends linearly on c and the thermodynamical force, which reduces to $\mathscr{F} = W^{(1)}(\overline{\mathbf{F}})$, is not affected by the damage variable c. Note that this very simple damage model, associated to the Voigt scheme, was the one already studied by Govindgee and Simo (1991) and extended in many variants by several authors Ogden and Roxburgh (1999) (for a pseudo-elasticity approach), Li et al. (2007), etc.

The next step is to specify the damage evolution law, that is the cavity growth process. For the coherence of the approach, this evolution law should be also deduced from micromechanical considerations. Since, until now, there is no theoretical or physical arguments to do this, the methodology followed here consists to combine the micromechanical approach with standard thermodynamic arguments related to the analysis of the intrinsic dissipation when damage phenomena occur. Indeed, noting that the positivity of the intrinsic dissipation reduces to $\mathscr{F}\frac{\partial c}{\partial t} \geqslant 0$, one postulates the existence of a dissipation pseudo-potential $\phi^*(\mathscr{F})$ as differentiable, convex, positive, zero for $\mathscr{F} = 0$ and such that:

$$\frac{\partial c}{\partial t} = \frac{\partial \phi^*}{\partial \mathscr{F}} \tag{19}$$

Following Devries and Brieu (1998) a Norton type form of the dissipation pseudo-potential is adopted:

$$\phi^*(\mathscr{F}) = \frac{\alpha}{\beta+1}\mathscr{F}^{\beta}, \quad \alpha \geqslant 0, \quad \beta \geqslant 0 \tag{20}$$

5.4. Implementation and results

Numerical implementation of the proposed damage model requires a simultaneous resolution of the homogenization problem and of the damage evolution. For this, we adopt a method separating the space problem that is the homogenization one and the temporal problem of damage evolution. Thus, the solution is obtained at a time t by continuity of two successive steps: for an initial porosity $c_0(t)$ and an imposed deformation gradient tensor $\overline{\mathbf{F}}(t)$, we compute $\widetilde{W}(\overline{\mathbf{F}}(t), c_0(t))$ and $\overline{\mathbf{T}}(\overline{\mathbf{F}}(t), c_0(t))$ by resolving the homogenization problem. After this, we evaluate the porosity $c_1(t)$ by the evolution law (19) and compute once again $\widetilde{W}(\overline{\mathbf{F}}(t), c_1(t))$ and $\overline{\mathbf{T}}(\overline{\mathbf{F}}(t), c_1(t))$. A convergence test is performed for the porosity (i.e $|c_1(t) - c_0(t)| \leqslant \varepsilon$ with ε very small); if the convergence is not obtained, we continue the successive steps in order to converge for an iteration $k : |c_k(t) - c_{k-1}(t)| \leqslant \varepsilon$. This method is analogous to one of Picard (see Burrage (1995)).

In this algorithm, presented in Fig. 14, the homogenization problem is solved as described previously in Section 3.1 and the

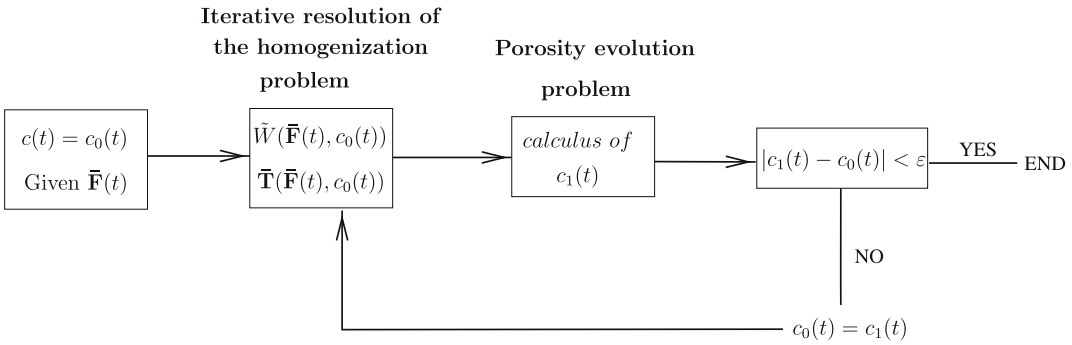

Fig. 14. Separation of the space problem and of the temporal problem.

porosity $c(t)$ is determined by the integration of the evolution law (19) based on (20):

$$c(t) = c(0) + \frac{\alpha\beta}{\beta+1}\int_0^t \mathscr{F}(t)^{(\beta-1)}dt \tag{21}$$

To compute $c(t)$, we choose to use a trapezoidal rule for integration. Thus, the damage evolution during a interval of time $[0,T]$ is determined by considering intermediate times t_j for which we compute the macroscopic stresses and the damage (porosity) of the material. These intermediate times are defined by $t_j = j\Delta t = j\frac{T}{N}(j = 1\ldots N)$, N being the number of sub-intervals in $[0,T]$ which have to be small enough for the desire accuracy. In summary, the evaluation of the porosity at each time t_j is then determined from the following approximation given by the trapezoidal rule:

$$c(t_j) = c_0 + \frac{\alpha\beta}{\beta+1}\left(\mathscr{F}(t_j)^{(\beta-1)} + 2\sum_{i=1}^{(j-1)}\mathscr{F}(i\Delta t)^{(\beta-1)}\right) \tag{22}$$

Let us consider now the composite EPDM/PP for which experimental data are available. It was shown in Bouchart et al. (2007) that a micromechanical model of composite, without damage, is not able to reproduce the macroscopic experimental behavior. Our objective here is simply to apply the damage model derived here to the EPDM/PP. Based on appropriate assumption of scales separation, the methodology followed consists in a two step homogenization: (i) we first homogenize the EPDM/PP in order to obtain its macroscopic behavior in absence of damage; (ii) we then consider this macroscopic behavior as the one of the solid matrix in the second homogenization step devoted to the damage modeling. In this second step of homogenization the initial porosity is considered very low (0.1%).

For the pseudo-potential ϕ^*, parameters α and β are calibrated on the data from the material made up of 90% of EPDM and 10% of PP particles: $\alpha = 1.10^{-4}\ s^{-1}$ and $\beta = 0.8$. Fig. 15(a) shows the results given by the damage model based on the Hashin–Shtrikman (HS) bound and the experimental data. It confirms the relevance of the identification. For completeness, the predictions of the model without damage phenomenon are also presented. A clear effect of the damage is observed and makes it possible to describe the experimental behavior.

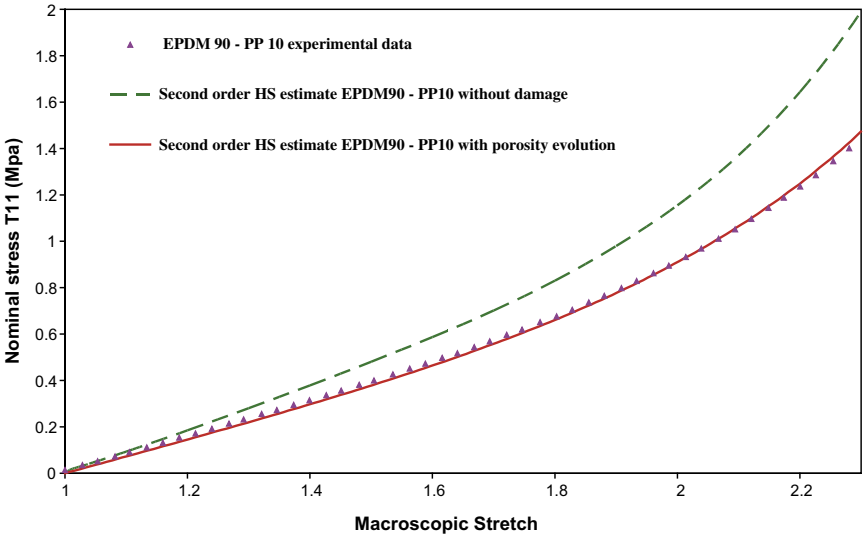

(a) HS-based model predictions with damage

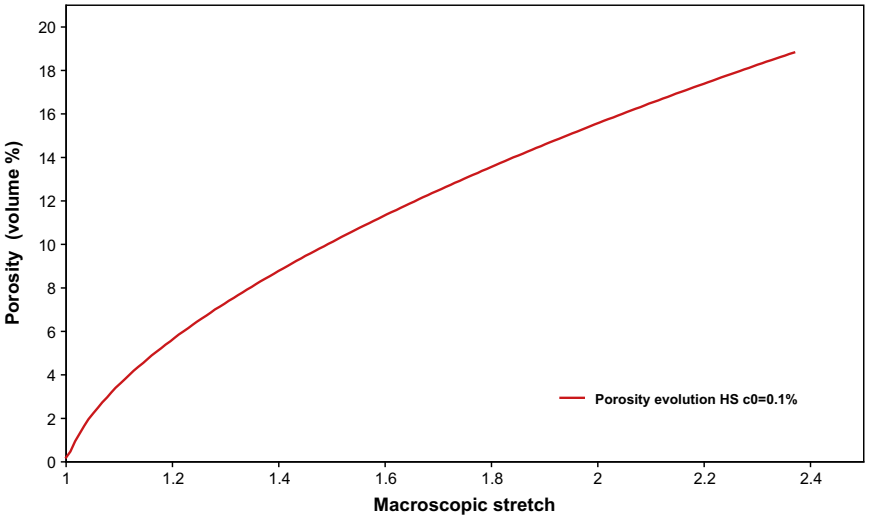

(b) Porosity evolution predicted by the HS-based model

Fig. 15. Verification uni-axial tensile test for the considered material with an initial porosity of 0.1%.

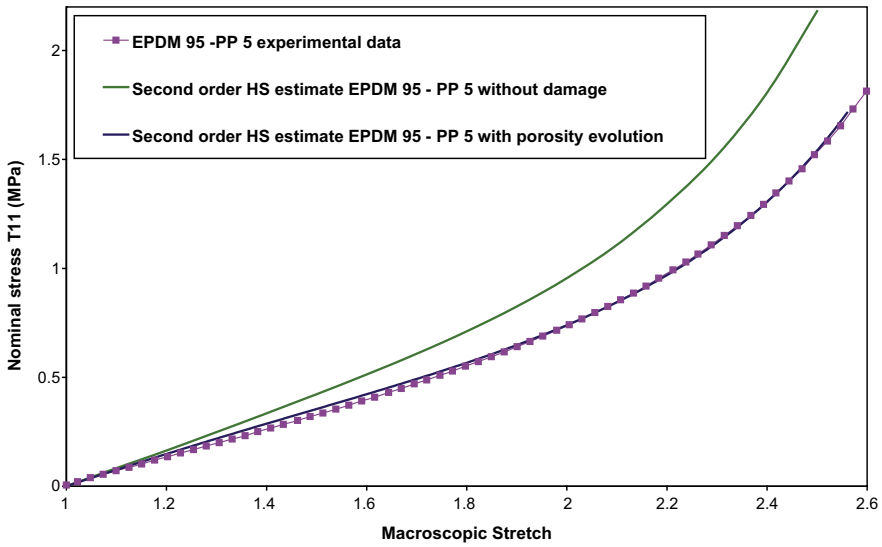

(a) HS-based model predictions with damage

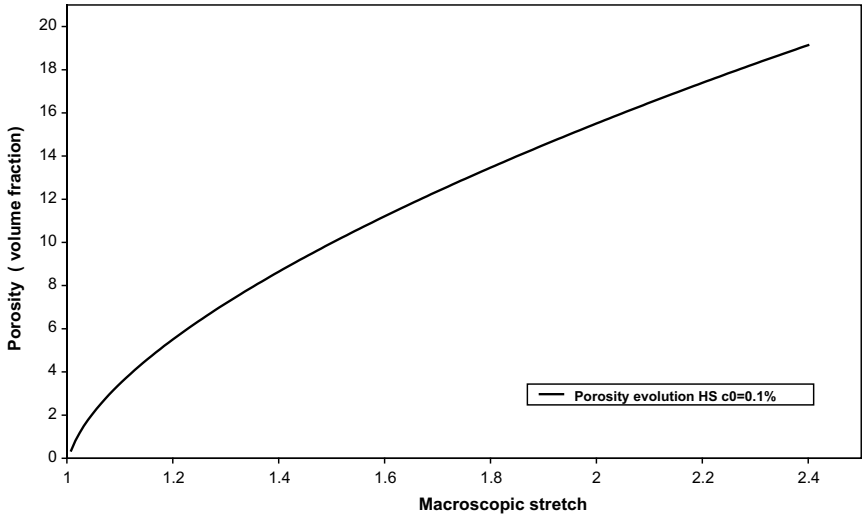

(b) Porosity evolution predicted by the HS-based model

Fig. 16. Validation uni-axial tensile test for the considered material with an initial porosity of 0.1%.

For validation purposes, another blend EPDM–PP made up now of 95% of EPDM and 5% of PP particles is considered. The comparison of the predictions to experimental data (see Fig. 16(a)) shows an agreement which demonstrates the predictive capabilities of the proposed model. The damage evolution during the loading is also presented in Figs. 15 and 16(b) for the two studied blends EPDM–PP. It is observed that for the maximum level of deformation in the test, the damage value is quite equal to 18%. For further details, one can refer to Bouchart (2007).

6. Conclusions

The present study is devoted to an experimental characterization and a multiscale modeling of the mechanical behavior of reinforced hyperelastic materials like EPDM/PP blends. The PP phase is assumed in the form of spherical particles embedded in the EPDM matrix. For the particles volume concentrations considered in the study, the experimental results show a significant effect of the reinforcements. The micromechanical modeling developped combines the second order homogenization method with an Hashin–Shtrikman bound. It leads to results in agreement with the reference solution obtained by FE computations. Comparisons of the HS-based model predictions with experimental data led us to extend the model by accounting of damage phenomena which occurs in the studied composite. Indeed, we had explored the effects of the presence and/or growth of microcavities in the EPDM/PP blends. The formulation of the damage model is obtained by combining the micromechanical results of the second order method with a standard thermodynamics-based approach. First validations of this damage model are then obtained through the comparison of its predictions with experimental data on the EPDM/PP. Works concerning the cyclic behavior of the damaged material are also under progress.

Appendix A. Jacobian matrix for the implementation of an hyperelastic strain energy density in Abaqus

The Jacobian matrix, $\mathbb{C}$, is defined by the variation of the Kirchhoff stresses:

$$\delta(J\boldsymbol{\sigma}) = J\mathbb{C}.\delta\mathbf{D} \tag{23}$$

where $\delta\mathbf{D}$ is the deformation rate, defined as the symmetric part of $\delta\mathbf{F}.\mathbf{F}^{-1}$.

The expression for the Cauchy stresses obtained by using, for example, the Lambert–Diani and Rey density (8) is the following:

$$\boldsymbol{\sigma} = \frac{2}{J}\left[e^{\left(\alpha_0+\alpha_1(I_1-3)+\alpha_2(I_1-3)^2\right)} + \beta_1 I_2^{\beta_2} I_1\right]\mathbf{B} - \frac{2}{J}\beta_1 I_2^{\beta_2}\mathbf{B}.\mathbf{B} \tag{24}$$

where $\mathbf{B} = \mathbf{F}\mathbf{F}^t$ is the left strain tensor of Cauchy–Green.

Thus, the expression of the variation of $J\boldsymbol{\sigma}$ is:

$$\begin{aligned}\delta(J\boldsymbol{\sigma}) = {} & 2\left[e^{(\alpha_0+\alpha_1(I_1-3)+\alpha_2(I_1-3)^2)} + \beta_1 I_2^{\beta_2} I_1\right]\delta\mathbf{B} \\ & + \mathbf{B}\left[e^{(\alpha_0+\alpha_1(I_1-3)+\alpha_2(I_1-3)^2)}(\alpha_1 + 2\alpha_2(I_1-3))\delta I_1 + \beta_1 I_2^{\beta_2}\delta I_1 + \beta_1\beta_2 I_2^{\beta_2-1} I_1\delta I_2\right] \\ & - 2\beta_1\beta_2 I_2^{\beta_2-1}\delta I_2\mathbf{B}.\mathbf{B} - 4\beta_1 I_2^{\beta_2}\delta\mathbf{B}\cdot\mathbf{B}\end{aligned}$$

It is necessary to determine the variations of $I_1,\ I_2$ and of $\mathbf{B}$ depending on $\delta\mathbf{D}$. For this, we use the Abaqus software manual (ABAQUS, 2004) which permits to determine the following variations of $\bar{I}_1 = J^{-2/3}I_1$, $\bar{I}_2 = J^{-4/3}I_2$ and $\overline{\mathbf{B}} = J^{-2/3}\mathbf{B}$:

$$\begin{aligned}\delta\overline{\mathbf{B}} &= \frac{1}{2}\left(\delta_{iq}\overline{\mathbf{B}}_{ip} + \delta_{ip}\overline{\mathbf{B}}_{jq} + \delta_{jq}\overline{\mathbf{B}}_{ip} + \delta_{jp}\overline{\mathbf{B}}_{iq} - \frac{4}{3}\delta_{pq}\overline{\mathbf{B}}_{ij}\right)\delta\mathbf{D}_{pq} \\ \delta\bar{I}_1 &= 2\left(\overline{\mathbf{B}}_{pq} - \frac{\bar{I}_1}{3}\delta_{pq}\right)\delta\mathbf{D}_{pq} \\ \delta\bar{I}_2 &= 2\left(\bar{I}_1\overline{\mathbf{B}}_{pq} - \frac{\bar{I}_1^2}{3}\delta_{pq} - \overline{\mathbf{B}}_{pm}\overline{\mathbf{B}}_{mq} + \frac{1}{3}tr(\overline{\mathbf{B}}.\overline{\mathbf{B}})\delta_{pq}\right)\delta\mathbf{D}_{pq}\end{aligned} \tag{25}$$

Then, we can compute the variations of I_1, I_2 and of $\mathbf{B}$ from those of $\bar{I}_1,\ \bar{I}_2$ and $\overline{\mathbf{B}}$:

$$\begin{aligned}&\delta\mathbf{B} = \tfrac{2}{3}(J^{-1/3}\delta J)\overline{\mathbf{B}} + J^{2/3}\delta\overline{\mathbf{B}} \\ &\delta I_1 = \tfrac{2}{3}(J^{-1/3}\delta J)\bar{I}_1 + J^{2/3}\delta\bar{I}_1 \\ &\delta I_2 = \tfrac{2}{3}(J^{1/3}\delta J)\bar{I}_2 + J^{4/3}\delta\bar{I}_2 \\ &\text{avec}\delta J = Jtr(\delta\mathbf{D}) = J(\mathbf{I}:\delta\mathbf{D})\end{aligned} \tag{26}$$

by replacing the expressions of $\delta\overline{\mathbf{B}}, \overline{\mathbf{B}}, \delta\bar{I}_1,\ \bar{I}_1$ and $\delta\bar{I}_2,\ \bar{I}_2$ and identifying with the definition of $\mathbb{C}$ (23), we obtained the expression of the Jacobian matrix.

References

ABAQUS, 2004. Abaqus Standard Theory Manual version 6.5. Hibbit, Karlson & Sorensen, Rhodes Isl.

Blatz, P., Ko, W., 1962. Application of finite elasticity to deformation of rubber materials. Trans. Soc. Rheol. 6, 223.

Bouchart, V., 2007. Etude expérimentale et modèlisation micromècanique du comportement et de l'endommagement des èlastoméres renforcès. PhD Thesis, Universitè des Sciences et Technologies de Lille, France.

Bouchart, V., Brieu, M., Kondo, D., Nant-Abdelaziz, M., 2007. Macroscopic behavior of a reinforced elastomer: micromechanical modelling, validation. Mèch. Ind. 8, 199–205.

Bouchart, V., Brieu, M., Kondo, D., Nant-Abdelaziz, M., 2008. Implementation, numerical verification of a nonlinear homogenization method applied to hyperelastic composites. Comp. Mater. Sci. 43–3, 670–680.

Brieu, M., Devries, F., 1999. Micro-mechanical approach and algorithm for the study of damage appearance in elastomer composites. Compos. Struct. 46–4, 309–319.

Burrage, K., 1995. Parallel, Sequential Methods for Ordinary Differential Equations. Clarendon Press, New York.

Ciarlet, P., Geymonat, G., 1982. Sur les lois de comportement en èlasticitè nonlinèaire incompressible. Comptes Rendus de l'Acadèmie des Sciences – Series II 295, 423–426.

Danielsson, M., Parks, D., Boyce, M., 2004. Constitutive modeling of porous hyperelastic materials. Mech. Mater. 36, 347–358.

Devries, F., Brieu, M., 1998. Approche micro/macro de l'endommagement de milieux èlastoméres. CRAS 326–12, 905–910.

Diani, J., Brieu, M., Gilormini, P., 2006a. Observation, modeling of the anisotropic visco-hyperelastic behavior of a rubberlike material. Int. J. Solid Struct. 43–10, 3044–3056.

Diani, J., Brieu, M., Vacher, J., 2006b. A damage directional constitutive model for mulins effect with permanent set, induced anisotropy. Eur. J. Mech. – A/Solids 25–3, 483–496.

Govindgee, S., Simo, J., 1991. A micro-mechanically bases continuum damage model for carbon black-filled rubbers incorporating mullins effect. J. Mech. Phys. Solids 39–1, 87–112.

Hashin, Z., Shtrikman, S., 1962. On some variational principles in anisotropic, nonhomogeneous elasticity. J. Mech. Phys. Solids 10–4, 335–342.

Hill, R., 1972. Convexity conditions, existence theorems in nonlinear elasticity. Arch. Rat. Mech. Anal. 63, 337–403.

Idiart, M., Ponte Castañeda, P., 2007. Field statistics in nonlinear composites. Part i. theory. Proc. R. Soc. Lond. A 463, 183–203.

Kakavas, P., 2002. Influence of the cavitation on the stress–strain fields of compressible blatz-ko materials at finite deformation. Int. J. Solid Struct. 39, 783–795.

Lahellec, N., Mazerolle, F., Michel, J., 2004. Second-order estimate of the macroscopic behavior of periodic hyperelastic composites: theory, experimental validation. J. Mech. Phys. Solids 52, 27–49.

Lambert-Diani, J., Rey, C., 1999. New phenomenological behavior laws for rubbers, thermoplastic elastomers. Eur. J. Mech. – A/Solids 18, 1027–1043.

Levin, V., 1967. Thermal expansion coefficients of heterogeneous materials. Mekh. Tverd. Tela 2, 93–94.

Li, J., Mayau, D., Lagarrigue, V., 2007. A constitutive model dealing with damage due to cavity growth, the mullins effect in rubber-like materials under triaxial loading. J. Mech. Phys. Solids doi:doi:10.1016/j.jmps.2007.06.009.

Llorca, J., Segurado, J., 2004. Three-dimensional multiparticle cell simulations of deformation, damage in sphere-reinforced composites. Mater. Sci. Eng. A 365 (1-2), 267–274.

Lopez-Pamies, O., Ponte Castañeda, P., 2007. Homogenization-based constitutive models for porous elastomers, implications for macroscopic instabilities: I. Analysis. J. Mech. Phys. Solids 55–8, 1677–1701.

Miehe, C., 1995. Discontinuous, continuous damage evolution in ogden-type large-strain elastic materials. Eur. J. Mech. – A/Solids 14–5, 697–720.

Mnllins, L., 1969. Softening of rubber by deformation. Rubber Chem. Technol. 42, 339–362.

Ogden, R., 1984. Nonlinear Elastic Deformations. Dover Publications Inc., New York.

Ogden, R., Roxburgh, D., 1999. A pseudo-elastic model for the mullins effect in filled rubber. Proc. R. Soc. Lond. A 455, 2861–2877.

Ponte Castañeda, P., 2002. Second-order homogenization estimates for nonlinear composites incorporating field fluctuations: Ii-applications. J. Mech. Phys. Solids 50–4, 759–782.

Ponte Castañeda, P., Suquet, P., 1998. Nonlinear composites. Adv. Appl. Mech. 34, 171–302.

Ponte Castaneda, P., 1996. Exact second order estimates for the effective mechanical properties of nonlinear composite materials. J. Mech. Phys. Solids 44, 827–862.

Ponte Castaneda, P., Tiberio, E., 2000. A second order homogenization method in finite elasticity, applications to black-filled elastomers. J. Mech. Phys. Solids 48, 1389–1411.

Press, W., Teukolsky, S., Vetterling, W., Flannery, B., 1992. Numerical recipes in fortran, the art of scientific computing, second ed. Cambridge University Press.

Willis, J., 1977. Bounds, self consistent estimates for the overall moduli of anisotropic composites. J. Mech. Phys. Solids 25, 185–202.